Evidence for global runoff increase related to climate warming

David Labat *, Yves Goddéris, Jean Luc Probst, Jean Loup Guyot

Laboratoire de Mécanisme de Transferts en Géologie, UMR CNRS/UPS 5563, 38, Rue des 36 Ponts, 31400 Toulouse, France

Abstract

Ongoing global climatic change initiated by the anthropogenic release of carbon dioxide is a matter of intense debate. We focus both on the impact of these climatic changes on the global hydrological cycle and on the amplitude of the increase of global and continental runoff over the last century, in relation to measured temperature increases. In this contribution, we propose an original statistical wavelet-based method for the reconstruction of the monthly discharges of worldwide largest rivers. This method provides a data-based approximation of the evolution of the annual continental and global runoffs over the last century. A consistent correlation is highlighted between global annual temperature and runoff, suggesting a 4% global runoff increase by 1 °C global temperature rise. However, this global trend should be qualified at the regional scale where both increasing and decreasing trends are identified. North America runoffs appear to be the most sensitive to the recent climatic changes. Finally, this contribution provides the first experimental data-based evidence demonstrating the link between the global warming and the intensification of the global hydrological cycle. This corresponds to more intense evaporation over oceans coupled to continental precipitation increase or continental evaporation decrease. This process finally leads to an increase of the global continental runoff.

Keywords: Climate change; Global runoff; Runoff-temperature relationship; Wavelet analysis

1. Motivations and objectives

Recent studies have shown that global mean temperature increases may have a serious impact on the global hydrological cycle at various spatial and temporal scales. A large and complete review of the most recent trends in hydrological changes related to global climate warming can be found in the IPPC 2001 report [18] [Chapter 4]. Two main effects are identified: increasing risk of floods [33] and droughts at local or regional scales and increase or decrease of water availability at the continental scale [43].

A large majority of these studies are based on outputs from simulations performed with GCMs or OAGCMs coupled to various distributed models of surface and subsurface hydrologic processes [13,32,34,35].

An alternative approach consists of an extensive analysis of the possible correlation between measured climate and hydrological parameters such as precipitation, runoff or temperature [10,12,24]. However, these studies usually deal with local or regional time series. Since Probst and Tardy's work [38,39], no recent global, data-based study has focused on possible global hydrological changes related to recent climate changes.

Powerful tools to perform such global and long term (10^1–10^2 years) analysis are the stream flows of large rivers draining 10^5–10^6 km^2, since they integrate rainfall, evaporation, topography, lithology, soil, and vegetation cover heterogeneities. However, the length and reliability of the available time series are highly variable. Moreover, gaps are usually found within the time series. Finally, the impact of dams or irrigation on the natural hydrological regime of rivers must be identified and anthropogenic effects must be removed. Such discrepancies between the various time series require the use of a pertinent method to complete or reconstruct runoff time series, prior to performing any analysis of global or continental long term runoff evolution. Then, in order to estimate missing runoff, we introduce a novel statistical wavelet method based on a reduced number of long-term large river runoff series. Wavelets are preferred to

* Corresponding author. Tel.: +33-561-52-86-85; fax: +33-561-52-05-44.

E-mail address: labat@lmtg.ups-tlse.fr (D. Labat).

classical correlation methods since they integrate the hydrological multi-scale variability.

2. Data

Previous studies of the global runoff fluctuations were based on a rather limited numbers of rivers [36,38,39]. In this contribution, the database is extended to 221 rivers: 66 North American rivers including the St. Lawrence, Colorado, Columbia, Ohio, Nelson and Mac Kenzie, 51 Asian rivers including the Mekong, Amur, Ob, Yenisey, Lena, Chang Jiang and Volga, 40 European rivers including the Danube, Northern Dvina and Elbe, 33 South American rivers including the Amazon, Parana, Orinoco and Tocantins and 31 African rivers including the Nile, Congo, Niger and Zambezi. The surface area of the gauging reference stations ranges from 10^4 to 4.5×10^6 km^2, latitude position ranges from 40.3 S to 72.37 N and longitude position ranges from –158.1 W to 184 E. Indeed, river discharges have been measured in some cases for only a few decades, while others have been sampled back to 1870. Sampling periods for the different rivers ranges from 4 to 182 years.

An exhaustive list of the selected rivers is given continent by continent in Tables 1–3. For each river, the watershed extend, the geographical localisation of the hydrometric station and the sampling interval are mentioned.

The Global Runoff Data Center and the Unesco River Discharge Database [42] provide most of the discharge data from selected rivers distributed all around the world (Fig. 1). Amazon discharges are provided by the Hybam Database (ANA, UNB, IRD). The most complete time series are available for North America and Europe.

A monthly sampling rate is used as it allows a precise study of the different time-scale fluctuations of the discharge of these large rivers, from monthly and seasonal to interannual fluctuations. This multi-scale behaviour of large river runoffs corresponding to multi-scale climate forcings justifies the introduction of a time-scale decomposition provided by wavelet methods [25,26].

Based on Baumgartner and Reichel estimations [2], the dataset roughly corresponds to 58% of the total African runoff, 46% of the total Asian runoff, 43% of the total European runoff, 44% of the total North American runoff, 80% of the total South American runoff, and 51% of the global runoff. By comparison, Probst et Tardy based their global reconstitution on 50 rivers corresponding to 13% of the global runoff.

3. Reconstruction method of the monthly river discharges

The key difficulty encountered in the analysis of the fluctuations in the runoff of large rivers is the multi-scale property of the signal in relation to several hydrological processes. Monthly fluctuations generally reflect the occurrence of low or high intensity events. Annual fluctuations record the variations of the annual water budget highlighting dry and humid years. *Multi-annual* fluctuations reflect the largest scale variations related to global general meteorological circulations and long term climate change. Among the different techniques widely used nowadays, wavelet and multi-resolution [11,16,29] analyses propose a time-scale transformation of the signal that accounts for flow variability. These methods have already been applied in different fields of hydrology ([9,14,22,23,25–27] and references therein).

4. Overview of the wavelet transform

The basic objective of the wavelet transform is to achieve a complete time-scale (or shift-scale) representation of localized and transient phenomena occurring at different time scales. In the wavelet transform, the Fourier basis is replaced by a two-parameter basis $\{\psi_{a,\tau}(t),(a,\tau)\in(R_+^*\times R)\}$ where "a" is the scale, and "τ" is time-shift. This allows a time-scale discrimination of processes. The coefficients of the wavelet transform of a continuous-time signal $x(t)$ are defined by the linear integral convolution operator:

$$C_x(a,\tau)=\int_{-\infty}^{+\infty}x(t)\psi_{a,\tau}^*(t)\,\mathrm{d}t \quad \text{with}$$
$$\psi_{a,\tau}(t)=\frac{1}{\sqrt{a}}\psi\left(\frac{t-\tau}{a}\right) \tag{1}$$

where $*$ corresponds to the complex conjugate. The function $\psi(t)$ is called a wavelet. The parameter "a" can be interpreted as a dilation ($a>1$) or contraction ($a<1$) factor of the wavelet function $\psi(t)$, corresponding to different scales of observation. The parameter "τ" can be interpreted as a temporal translation or shift of the function $\psi(t)$, which allows the study of the signal $x(t)$ locally around the time τ. Actual hydrological signals are discrete in time. Then, both the time shift (τ) and the "scale" domain ("a") are also discretized. The discretized version of Eq. (1) defines the discrete wavelet transform coefficients as follows:

$$C_x(j,k)=\int_{-\infty}^{+\infty}x(t)\psi_{j,k}^*(t)\,\mathrm{d}t \quad \text{with}$$
$$\psi_{j,k}(t)=a_0^{j/2}\psi(a_0^j t-k\tau_0) \tag{2}$$

where $*$ corresponds to the complex conjugate. The integer "j" is the scale factor, analogous to the "a" parameter of Eq. (1) and the integer "$k\tau_0$" is the translation factor analogous to the "τ" parameter. If one takes $a_0=2$ and $\tau_0=1$, the continuous scale-time grid is replaced by a discrete dyadic grid of the form: $(\{2^{-j},k.2^{-j}\},\ (k,j)\in Z^2)$. The orthogonal discrete wavelet transform coefficients $C_{j,k}$ are then defined by the convolution product:

Table 1
Name, watershed area, geographical localisation and discharge series extend of the selected rivers over Africa (Panel A) and Asia (Panel B)

River	Area	Lat	Long	From	To
Panel A: Africa					
Nile	2,870,000	23.96	32.90	1870	1980
Senegal	268,000	16.52	−15.5	1952	1989
Niger	1,000,000	11.87	3.38	1953	1980
Congo-Zaire	3,475,000	−4.3	15.3	1903	1984
Tana	42,217	−0.45	39.70	1934	1976
Sanaga	131,520	3.76	10.07	1944	1980
Oranje	850,530	−28.71	17.73	1965	1987
Zambezi	940,000	−16.15	33.58	1976	1980
Moulouya	24,422	34.24	−3.32	1959	1989
Rufiji	158,200	−7.8	37.92	1955	1963
Ogooue	203,500	0.68	10.23	1954	1976
Volta	394,100	6.2	0.10	1936	1964
Save River	100,885	−21.1	34.68	1976	1980
Limpopo	342,000	−24.54	33.00	1976	1980
Shebele	272,700	2.37	45.42	1954	1970
Nyong	26,400	3.57	10.12	1951	1977
Mangoky	53,225	−21.83	43.87	1965	1976
Cavally	28,800	4.38	−7.59	1971	1997
Bandama	95,500	5.88	−4.75	1970	1997
Sassandra	62,000	5.76	−6.60	1977	1997
Comoe	69,900	6.28	−3.49	1970	1988
Kouilou	55,010	−4.1	12.07	1969	1983
Benue	107,000	9.25	12.50	1960	1990
Incomati	37,600	−25.02	32.73	1976	1980
Maputo	28,500	−26.78	32.43	1976	1980
Shire	149,500	−16,549	35.13	1953	1982
Pangani	25,110	−5.17	38.47	1971	1979
Tugela	28,920	−29,139	31.39	1965	1973
Oueme	46,990	6.90	2.45	1963	1981
Juba	179,520	3.56	42.32	1951	1968
Panel B: Asia					
Mekong	391,000	16.53	104.73	1925	1987
Godavari	299,320	16.92	81.78	1902	1961
Indigirka	305,000	69.58	147.35	1937	1992
Kamchatka	51,600	56.27	161.67	1941	1988
Ural	308,000	50.85	51.28	1921	1985
Amur	1,730,000	50.63	137.12	1933	1985
Ob	2,430,000	66.57	66.53	1930	1995
Yenisey	2,440,000	67.48	86.50	1936	1996
Maya	165,000	59.75	134.75	1965	1985
Kolyma	361,000	67.37	153.67	1934	1958
Lena	2,460,000	72.37	126.80	1951	1995
Yana	216,000	69.77	135.23	1938	1985
Alazeja	29,000	69.17	154.50	1978	1994
Bramaputra	636,130	25.18	89.67	1972	1976
Chang Jiang	1,705,383	30.76	117.62	1950	1987
Ganges	935,000	25	87.92	1965	1974
Huang He	730,036	34.92	113.65	1949	1989
Indus	832,418	25.37	68.37	1975	1980
Krishna	251,355	16.52	80.62	1901	1961
Mahanadi	132,090	20.42	83.67	1965	1971
Narmada	89,345	21.92	73.65	1949	1961
Penzhina	71,600	62.42	166.03	1968	1985
Pur	95,100	67.00	78.22	1939	1978
Xi Jiang	329,705	23.48	111.30	1946	1985
Nadym	48,000	65.62	72.67	1968	1992
Taz	100,000	66.59	82.28	1962	1984
Olenek	198,000	72.12	123.22	1953	1991
Anabar	78,500	71.98	193.95	1966	1995
Anadyr	47,300	65.08	169.00	1965	1985
Volga	1,360,000	48.77	44.72	1879	1936

(*continued on next page*)

Table 1 (*continued*)

River	Area	Lat	Long	From	To
Yongding	42,500	40.23	115.60	1949	1956
Luanhe	44,100	39.73	118.75	1946	1989
Huaihe	121,330	32.93	117.38	1950	1987
Beijiang	34,013	23.85	113.27	1954	1988
Dongjiang	25,325	23.17	114.30	1960	1988
Irrawady	117,900	21.97	96.1	1978	1989
Karkheh	45,882	31.47	48.42	1976	1980
Euphrates	274,100	32.72	44.27	1965	1973
Tigris	134,000	33.3	44.38	1965	1973
Han	25,046	37.52	126.97	1955	1973
Mahi	33,670	22.3	73.03	1968	1980
Tapi	61,575	21.28	72.95	1965	1980
Penner	53,290	14.45	79.98	1965	1975
Cauvery	74,000	10.83	78.83	1976	1980
Omoloy	108,000	69.38	134.62	1979	1994
Syr-Darya	219,000	44.05	67.05	1949	1985
Amu-Darya	450,000	42.28	59.70	1938	1974
Chao Praya	110,569	15.67	100.12	1976	1994
Chindwin	27,420	26	95.70	1978	1989
Karun	60,769	31.32	48.67	1965	1971
Bol Anui	49,600	68.15	161.17	1978	1989

$$C^{x}_{j,k} = \int_{-\infty}^{+\infty} x(t)\psi^{*}_{j,k}(t)\,\mathrm{d}t \quad \text{with}$$
$$\psi_{j,k}(t) = 2^{j/2}\psi(2^{j}t - k) \tag{3}$$

To sum up, the multi-resolution analysis allows an orthogonal decomposition of a sampled hydrological signal in term of approximation and details of increasing order of resolution.

5. Reconstruction method

The proposed global and continental runoff reconstruction is based on reference runoff series selected among the overall database in relation to their high reliability over long period (several decades). Anthropogenic effects are first removed by truncation. For instance, *Nile* discharges after Assam Dam construction are removed. It should be noted that these reference series consist in a reduced number of ten reference rivers.

The multi-resolution analysis of river discharge series is based on a Daubechies D20 wavelet, since this wavelet constitutes in general the optimal orthogonal wavelet representation for runoff series [25,26]. The multi-resolution is implemented using classical multi-resolution MATLAB algorithm described in [25,26].

The multi-resolution analysis of the reference runoff series defines three ''hydrological'' reference components (month, annual and *multi-annual*). For example, the annual component corresponds to the classical recharge–discharge process. Then, for each rivers, a three-step reconstruction method estimates missing monthly runoffs.

The first step identifies the three ''hydrological'' components (month, annual and *multi-annual*) through multi-resolution analysis of each non-reference runoff series. For each hydrological component, the second step consists in the determination for each time series of the reference river characterized by as similar as possible fluctuations, possibly delayed in time. The maximum of the cross-correlation function between the considered runoff series and each reference rivers are calculated. The ''optimum'' reference river and the ''optimum'' delay for each scales (month, annual and pluri-annual) corresponds to the highest cross-correlation value. The missing values are estimated in a third step. For each time-scale component, missing values are estimated using a linear regression with the ''optimum'' reference river. The summation of the three components leads to an estimation of the reconstructed discharges. This method provides a qualitative reconstruction of the runoff's temporal structure. To provide both similar temporal variability and frequency distributions between the reconstructed and the observed time series, mean, variance and probability density distribution are calibrated on to the observed values.

At monthly scales, mean correlation coefficients are respectively 0.45 and −0.37. That indicates that a simple regression analysis based on monthly runoffs may lead to poor results. At large scales, mean correlation coefficients are respectively 0.48 and −0.39. Finally, the main improvement of this method compared to a simple regression analysis lies in the quality of the annual components rivers reconstruction (Fig. 2). Mean annual correlation coefficients are respectively 0.8 and −0.78 with a maximum of correlation observed at the highest latitudes.

Table 2
Name, watershed area, geographical localisation and discharge series extend of the selected rivers Europe

River	Area	Lat	Long	From	To
Garonne	52,000	44.42	0.23	1921	1980
Loire	110,000	47.38	−0.83	1863	1980
Guadalquivir	46,995	37.52	−5.98	1913	1964
Seine	44,320	48.83	2.27	1928	1965
Rhone	95,590	43.92	4.67	1921	1980
Ebre	84,230	40.82	0.52	1913	1965
Vuoksi	61,275	61.15	28.78	1847	1985
Elbe	131,950	5.24	10.89	1875	2000
Vistule	194,376	54.09	18.82	1901	1994
Oder	109,729	52.76	14.32	1901	1994
Danube	807,000	45.18	28.73	1921	2000
Jucar	17,876	39.11	−0.65	1913	1966
Tiber	16,545	41.9	12.48	1921	1980
Western Dvina	64,600	55.88	26.68	1965	1985
Po	70,091	44.88	11.65	1918	1986
Rhine	159,680	51.76	6.40	1854	2000
Vannern-Gota	46,830	58.38	12.32	1807	1966
Weser	37,790	52.96	9.13	1857	2000
Dnestr	66,100	46.8	29.37	1965	1985
Dnieper	463,000	47.92	35.15	1952	1985
Drava	37,142	45.78	18.20	1921	1974
Mezen	56,400	65.00	45.62	1921	1994
Northern Dvina	348,000	64.1	42.17	1882	1994
Neva	281,000	59.8	30.72	1859	1989
Don	378,000	47.5	40.67	1891	1953
Kemi	50,790	65.95	24.7	1911	1985
Kymijoki	36,535	60.8	26.82	1939	1993
Glomma	10,243	59.36	11.07	1902	1973
Neman	81,200	55.01	22.52	1812	1994
Petchora	248,000	65.42	52.28	1932	1985
Douro	91,491	41.15	−7.68	1933	1969
Tejo	67,490	39.47	−8.37	1976	1982
Guadania	60,833	37.82	−7.63	1948	1990
Angerman	30,640	63.17	17.27	1965	1999
Kokemkenjoki	26,025	61.35	22.12	1931	1993
Kenijoki	50,900	65.78	24.55	1949	1993
Narva	56,000	59.35	28.25	1956	1992
Southern Bug	46,200	47.72	31.18	1965	1985
Kuban	48,100	45.15	38.32	1965	1985
Kura	178,000	40.12	48.67	1930	1985

Reconstructed discharge time series are summed up continent by continent and a weighting coefficient based on the estimation of global and continental mean annual performed by Baumgartner and Reichel is applied to account for the complete continental surface. Finally, estimation of the global runoff is achieved by applying a 1/0.89 coefficient to account for the Australian and Antarctic continents contribution.

6. Variability of the reconstructed global runoffs

''Year to year'' mean fluctuations of the reconstructed continental runoffs display a succession of dry and humid periods (Fig. 2). African runoff is characterized by a long dry period from 1900 to 1960 contrasting with intense humid periods occurring around 1890 and 1965. Asian runoff shows a periodic succession of dry and humid periods. This 15 year periodic signal presents a constant 10-year delay with the African runoff. North American runoff is characterized by a dry period between 1910 and 1940 followed by a regular succession of 10-year long humid and dry periods. This pattern shows also a rough 10-year shift compared to European runoff for the 1920–1980 period. South American runoff displays a rapid succession of dry and humid periods for the 1890–1945 interval. North American and Asian runoff exhibit similar fluctuations, roughly in opposition with the European behaviour. African and South American continental runoff appear as quite disconnected from others signals for the complete reconstruction period.

Global runoff fluctuations show a long dry period between 1900 and 1940 followed by a succession of

Table 3
Name, watershed area, geographical localisation and discharge series extend of the selected rivers over North America (Panel A) and South America (Panel B) ans Australia (Panel C)

River	Area	Lat	Long	From	To
Panel A: North America					
St. Lawrence	764,600	45.01	−74.79	1861	1984
Red River	104,000	49	−97.22	1913	1985
Assiniboine	153,000	49.86	−97.40	1913	1985
North Saskatchewan	131,000	53.2	−105.77	1912	1985
South Saskatchewan	141,000	52.13	−106.65	1912	1970
Susquehanna	62,419	40.25	−76.88	1891	1984
Niagara	686,000	43.15	−79.05	1860	1985
San Pedro	25,800	21.97	−105.15	1976	1981
Fuerte	34,247	25.95	−109.05	1976	1982
St. Marys	210,000	46.51	−84.37	1860	1911
Winnipeg	126,000	50.22	−95.57	1908	1985
Colorado River	289,562	36.86	−111.59	1911	1966
Mississippi	444,185	38.88	−90.18	1928	1985
Ohio	525,770	37.15	−88.74	1928	1985
Columbia	613,830	45.61	−121.17	1879	1974
Yaqui	57,908	28.93	−109.62	1976	1980
Hudson	20,953	42.75	−73.69	1947	1984
Delware	17,560	40.21	−74.78	1913	1985
Potomac	29,940	38.96	−77.12	1931	1985
Alabama	56,980	31.53	−87.52	1931	1960
Yukon	264,000	64.06	−139.43	1966	1996
Nelson	1,000,000	54.76	−97.92	1966	1985
Bravo	459,902	25.9	−97.52	1976	1980
Athabasca	133,000	56.78	−111.4	1966	1985
Miles lles	146,000	45.54	−73.87	1927	1961
Panuco	58,115	21.98	−98.57	1965	1980
Santiago	122,960	21.82	−105.12	1965	1982
Usumacinta	47,697	17.43	−91.5	1969	1984
Back	93,900	66.08	−96.5	1965	1997
Fraser	217,000	49.38	−121.45	1913	1997
MacKenzie	1,570,000	65.28	−126.85	1966	1997
Moose river	60,100	50.81	−81.3	1966	1985
Slave River	606,000	59.86	−111.58	1960	1985
Stikine River	29,300	57.9	−131.15	1965	1985
Altamaha	35,224	31.65	−81.83	1932	1985
Apalachicola	44,548	30.7	−84.86	1930	1985
Brazos	116,568	29.58	−95.76	1923	2000
Copper	53,354	61.46	−144.45	1956	1985
Klamath	31,339	41.51	−124	1951	1995
Kuskowim	80,549	61.86	−158.1	1952	1994
Susitna	50,246	61.54	−150.51	1975	1993
Quachita	39,622	32.5	−92.13	1965	1976
San Joaquim	35,058	37.67	−121.26	1930	2000
Connecticut	25,019	41.98	−72.6	1929	2000
Nueces	43,149	28.04	−97.86	1940	2000
Trinity	44,512	30.43	−94.85	1925	2000
Skeena	42,200	54.63	−128.43	1939	1997
Peel River	70,600	67.25	−134.88	1975	1994
Anderson River	56,300	68.63	−128.41	1970	1994
Baleine River	43,200	55.28	−77.58	1963	1993
Melezes River	42,700	57.67	−69.61	1963	1982
Thelon River	65,300	64.53	−101.4	1972	1997
Attawapiskat	36,000	53.1	−87.08	1968	1994
Kazan River	72,300	63.65	−95.85	1972	1997
Winisk	50,000	54.52	−87.23	1983	1995
Albany River	118,000	51.33	−83.87	1972	1995
Grande Riviere	96,300	53.73	−78.57	1960	1978
Savannah	25,511	32.53	−81.26	1938	2000
River aux Feuilles	41,700	58.64	−70.42	1963	1987
Riviere George	35,200	58.15	−65.84	1963	1970
Quoich River	30,100	64.31	−93.9	1972	1980

Table 3 (*continued*)

River	Area	Lat	Long	From	To
Seal River	48,100	58.89	−96.27	1955	1988
Severn River	94,300	55.37	−88.32	1983	1995
Nottaway	57,500	50.13	−77.41J	1961	1982
Rupert	40,900	51.45	−76.87	1964	1995
Eastmain	44,300	52.25	−78.07	1960	1980
Panel B: South America					
Parana	2,300,000	−27.46	−58.85	1905	1983
Sab Francisco	510,800	−9.41	−40.52	1929	1980
Amazonia	4,500,000	−1.91	−55.50	1903	1998
Paraiba do Sul	55,083	−21.75	−41.33	1928	1992
Magdalena	257,438	10.26	−74.92	1976	1980
Uruguay	249,312	−31.95	−58.02	1969	1980
Tocatins	727,900	−5.13	−49.35	1970	1982
Negro	95,000	−40.43	−63.67	1973	1980
Jequitinhonha	62,365	−16.13	−40.3	1943	1979
Rio Parnaiba	282,000	−3.43	−42.5	1976	1982
Orinoco	836,000	8.14	−63.6	1925	1990
Salado	40,000	−26.22	−63.75	1935	1980
Jachal	25,500	−30.22	−68.83	1937	1980
San Juan	25,000	−31.52	−68.63	1910	1980
Rio Prado	30,360	−15.57	−39.28	1937	1970
Cuyuni	53,400	6.43	−58.82	1973	1982
Essequibo	66,600	5.84	−58.58	1965	1992
Corantijn	51,600	5.8	−57.12	1973	1980
Maroni	63,700	4.98	−54.43	1976	1980
Negro	63,000	−33.12	−57.18	1952	1980
Oyapock	25,120	3.82	−51.88	1954	1996
Xingu	446,570	−3.2	−52.22	1972	1995
Rio Jari	51,345	−0.68	−52.55	1973	1986
Rio Paru de Este	30,945	−0.42	−53.7	1973	1989
Rio Capim	38,178	−2.51	−47.82	1972	1987
Rio Gurupi	31,850	−1.83	−46.22	1974	1986
Rio Pindare	34,300	−3.66	−45.46	1972	1992
Rio Mearim	25,500	−4.21	−44.76	1976	1992
Rio Itapecuru	50,800	−3.63	−44.38	1969	1992
Rio Parnaiba	322,823	−3.45	−42.37	1982	1993
Rio Jaguaribe	48,200	−5.219	−38.2	1967	1983
Rio Paraguacu	31,488	−12.52	−39.87	1967	1979
Rio de Contas	42,245	−13.88	−40.1	1954	1978
Rio Tapajos	358,657	−6.03	−57.6	1985	1995
Panel C: Australia					
Burdekin	129,660	−19.76	147.24	1951	1993
Fitzroy	136,650	−23.14	150.37	1915	1951
Mitchell	46,050	−18.95	142.38	1973	1988
Murray	991,000	−34.18	141.6	1973	1985
Emu Spring	82,300	−27.85	114.54	1968	1997
Nune Mile	73,400	−24.82	113.77	1958	1997
Nanutarra	70,200	−22.54	115.489	1973	1996
Jimbegnyinoo	48,900	−21.32	116.15	1969	1995
Coolenar	49,600	−20.31	119.235	1975	1995
Coolibah	44,900	−15.52	130.945	1970	1996

15-year long dry and humid periods. A 65–70 year-long term process is also identified [40]. Compared to previous estimates this global runoff reconstruction displays more pronounced amplitudes of dry and humid periods.

In order to compare our results with previous study [38,39] which focused over the 1900–1975 period, trends have been calculated for two reference periods: 1900–1975 and 1925–1994 so that recent changes corresponding to the recent increase in temperature are emphasized (Fig. 3).

Effectively, over the first period, the linear regression between global runoff (R_{GLOBAL} in 10^{16} l/year) versus time lead to $R_{\mathrm{GLOBAL}} \propto 41.47 \times 10^{-5}$ t, whereas on the second period $R_{\mathrm{GLOBAL}} \propto 112.24 \times 10^{-5}$ t.

Global *runoff values* exhibit the same increase as mentioned in [38,39] for the 1900–1975 period (mean

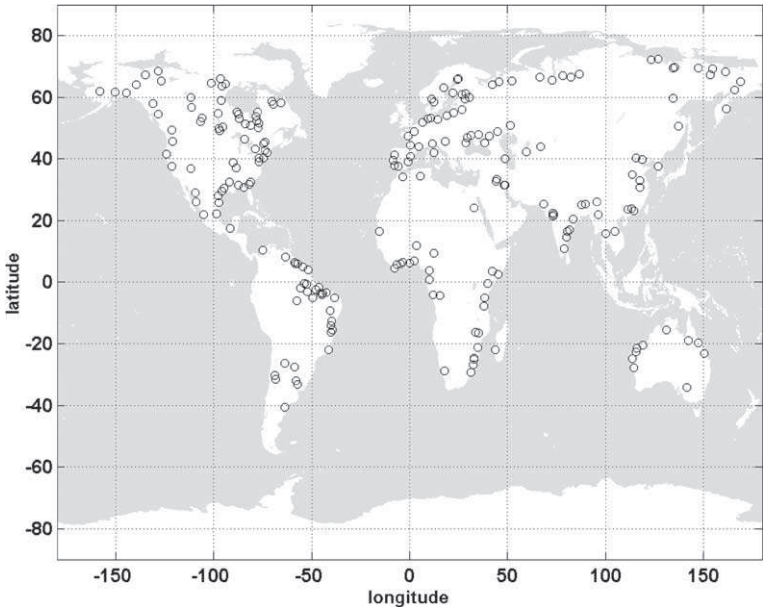

Fig. 1. Geographical location of the 231 stations considered in the continental and global runoff reconstruction process. Spatial repartition of the gauging stations appears homogeneous and globally follows the latitudinal distribution of continents, given that 46 rivers are located in the southern hemisphere and 185 rivers in the northern hemisphere. Surface area of the gauging reference stations ranges from 10^4 to 4.5×10^6 km^2, latitude and longitude position ranges respectively from 40.3 S to 72.37 N and −158.1 W to 184 E.

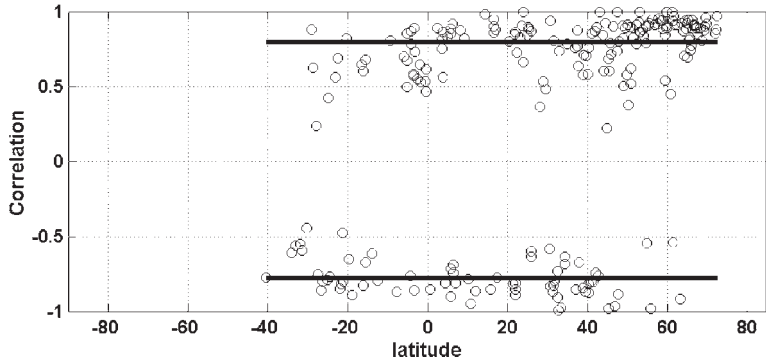

Fig. 2. Statistical validation of the wavelet-reconstruction of annual discharge fluctuations: latitudinal distribution of the correlation coefficient between measured discharges and wavelet reconstructed discharge series. Mean annual correlation coefficients are respectively 0.8 and −0.78 with a maximum of correlation observed at the highest latitudes.

increase of 1.68×10^{11} l/year in [38,39] compared to 1.84×10^{11} l/year in the present contribution) but the second period is characterized by a more rapid increase with an increasing rate multiplied by 3, largely driven by the North American and Asian runoff changes.

At the regional scale, on the first interval (1900–1975), our results are also in accordance with linear regression obtained in [38,39]. Focusing on the 1925–1994 time interval (where most of the global temperature increase occurred) global and continental normalized runoffs (R in 10^{16} l/year) are characterized by the following trends:

$$\begin{aligned} R_{\mathrm{AFRICA}} &\propto 25.79\times10^{-5}\ \mathrm{t}\\ R_{\mathrm{ASIA}} &\propto 152.89\times10^{-5}\ \mathrm{t}\\ R_{\mathrm{EUROPE}} &- 28.98\times10^{-5}\ \mathrm{t}\\ R_{\mathrm{N.\,AMERICA}} &\propto 204.81\times10^{-5}\ \mathrm{t}\\ R_{\mathrm{S.\,AMERICA}} &\propto 96.45\times10^{-5}\ \mathrm{t} \end{aligned} \tag{4}$$

where t is time in years.

Slight differences between the two reference periods are found for European runoff (stabilisation but still decrease) and South American runoff. African *runoff* increases rapidly during the first period, and tends to be constant during the second period. The increasing rate of

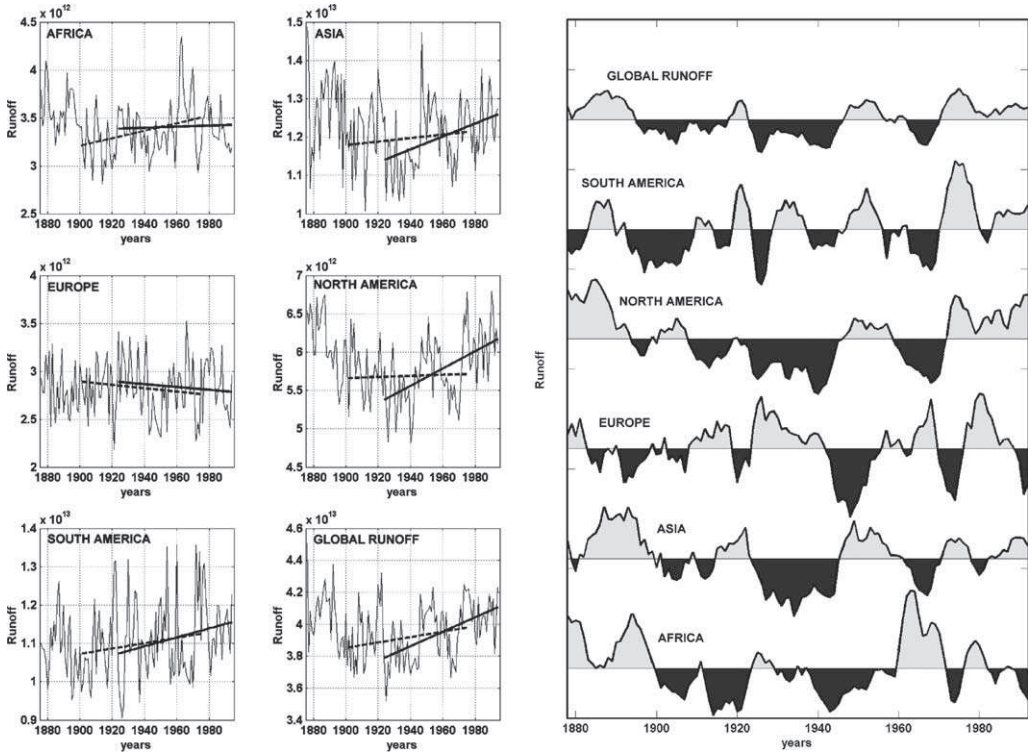

Fig. 3. *Left*: Mean annual runoffs (in l/s) for the five continents and linear regressions for 1900–1970 and 1925–1994 intervals. Note that except for the African and European continents, mean annual runoffs increase more rapidly during the second period, itself corresponding to a rapid global warming. (Normalized regression coefficients of runoff fluctuation versus time for the 1900–1970 and 1925–1994 periods are respectively 0.390 and 0.058 for African runoffs, 0.459 and 1.692 for Asian runoff, −0.175 and −0.147 for European runoff, 0.071 and 1.128 for North American runoff, 0.701 and 1.167 for South American runoff, 1.668 and 4.517 for global runoff.) *Right*: 3 year moving average of mean-averaged normalized continental and global runoffs showing the succession of dry (dark gray) and humid (light gray) periods (from bottom to top: Africa, Asia, Europe, North America, South America and Global runoffs). Note the existence of a constant shift or opposition between the different continental runoff fluctuations.

Asian runoff, which greatly contributes to global runoff is multiplied by 3 from the first reference period to the second one. Finally, North American runoff behaviour widely changes from the first to the second period: the relative stability observed during the first period is followed by a rapid increase for the second period.

7. Relation between global runoff and temperature

Global temperatures are estimated from a common combination of land air temperature anomalies and sea surface temperature anomalies [19–21]. The runoff-temperature relationship exhibits a global positive correlation. Indeed, the 1875–1925 temperature decrease is correlated with global runoff decrease over the same interval. Then, this tendency is inverted over the second interval (1925–1994). Moreover, a 15 year shift is observed between temperature and runoff response (Fig. 4).

The regression coefficient between temperature and runoff can be expressed in two ways: a simple ratio between temperature and runoff increase versus time or a linear regression between annual mean temperature and runoff. Using an incremental method, the following relationship holds between runoff and temperature temporal increases:

$$\delta R_{\mathrm{GLOBAL}} = 0.245\ \delta T_{\mathrm{GLOBAL}} \tag{5}$$

However, this relationship integrates all the fluctuations of both global temperature and runoff signals, and does not discriminate between yearly fluctuations and the *long-term* trends. Therefore, a linear regression between annual global runoff and annual global temperature was performed for the 1926–1994 period, leading to the following relationship:

$$R_{\mathrm{GLOBAL}} \propto 0.039\ T_{\mathrm{GLOBAL}} \tag{6}$$

In order to validate the statistical significance of this slope, a *Student* test is operated. The *Student* test consists in a test of *non-null linear* regression coefficient against null hypothesis. The null hypothesis implies no relationship between variables. The corresponding t-statistics is defined as the ratio between slope and standard error on the slope. This t-statistic will be large and positive if the slope is significantly greater than zero and large and negative is the slope is significantly less than zero. For example, with 10 degrees of freedom, a t-statistic of 8 or greater occurs 0.0006% of time. In the runoff-temperature

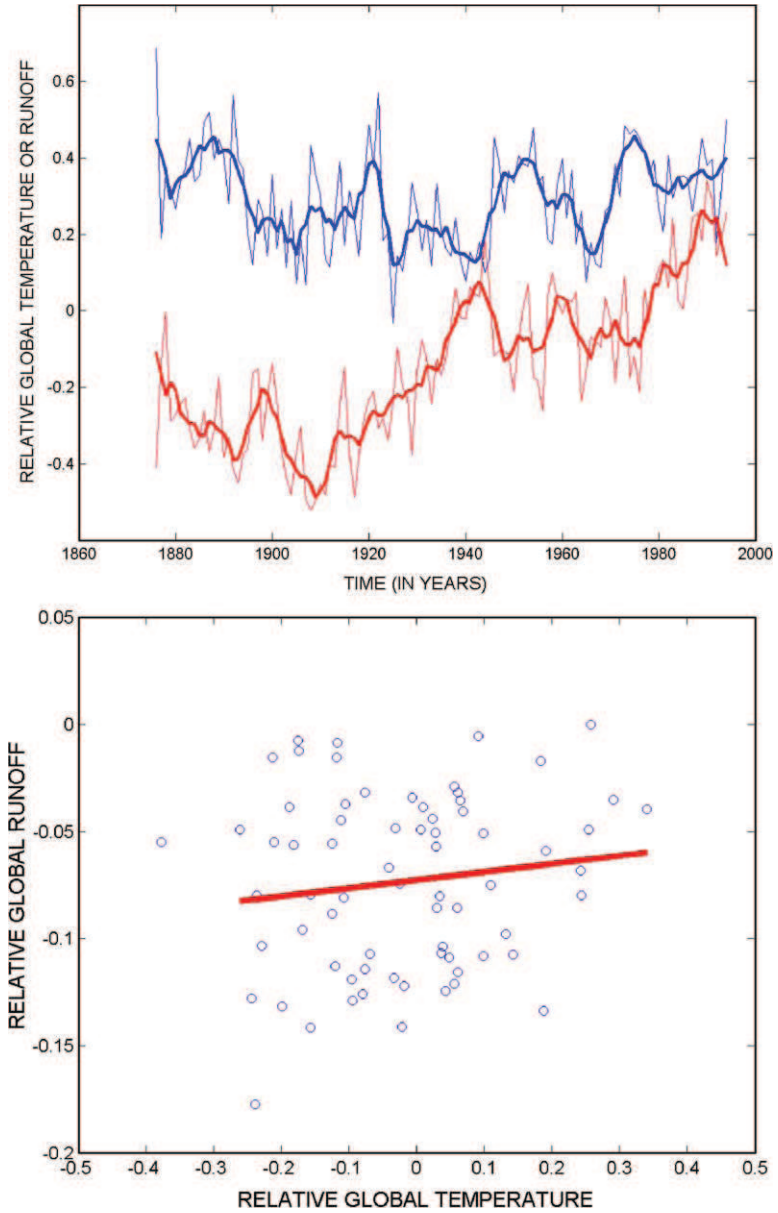

Fig. 4. *Top*: Annual global temperature (red) and global runoff (blue) fluctuations over the 1875–1994 period. Five year moving average of both signals are superimposed in order to highlight the general tendency. Note the existence of both periods: a conjugated decrease of temperature and runoff over the 1875–1910 period followed by a conjugated increase of both signals over the 1925–1994 period. There is a 15 years shift in the global hydrological response to global warmer conditions. *Bottom*: Global temperature versus global runoff relationship over the 1925–1994 period. The linear regression is characterized by a 0.039 slope significantly different from zero (T-student test equal to 12.45). (For interpretation of the references of colour in this figure legend, the reader is referred to the web version of this article.)

relationship, this slope differs significantly from zero with a T-student test equal to 12.4. Indeed, the following relationships hold at continental scale:

$$
\begin{aligned}
&R_{\text{AFRICA}} \propto -0.062\ T_{\text{NORTH}}\\
&R_{\text{AFRICA}} \propto -0.059\ T_{\text{SOUTH}}\\
&R_{\text{ASIA}} \propto 0.088\ T_{\text{NORTH}}\\
&R_{\text{EUROPE}} \propto 0.078\ T_{\text{NORTH}}\\
&R_{\text{N. AMERICA}} \propto 0.110\ T_{\text{NORTH}}\\
&R_{\text{S. AMERICA}} \propto 0.057\ T_{\text{SOUTH}}
\end{aligned}
\qquad (7)
$$

All slopes differ significantly from zero with *Student* test superior to 10. These correlations might be positive or negative at the continental scale, which indicates the high complexity of the feedback of temperature increase on the hydrological cycle at the regional scale.

8. Discussion of results

These hydrological fluctuations accompany an increase of CO_2 concentrations in the atmosphere. The

investigation of the relationship between runoff and CO_2 or temperature is of high importance for understanding past palaeoclimates of the Earth [6,37] but also for forecasting ongoing changes to the hydrological cycle [1,8].

In paleoclimate models, the amplitude of past atmospheric CO_2 fluctuations is strongly dependent on the ability of global continental silicate weathering (acting as a sink of CO_2) to counteract changes in the volcanic CO_2 emission. As previously suggested [7,17,44], continental silicate weathering increases when temperature increases, providing the mathematical expression for the negative feedback required to stabilize atmospheric CO_2 (a greenhouse gas) and climate at the geological timescale (33–35). Global silicate weathering is generally assumed to increase with global runoff, itself assumed to be more efficient under warmer conditions. The relationship between global temperature and global runoff included in the GEOCARB [3–5] model postulates a 3.8% increase in runoff per °C. This relationship is based on the results of rather old simulations performed with climatic models [15,30,31]. In this contribution, we experimentally demonstrate the validity of the runoff-temperature relationship of the GEOCARB model considering a global temperature increase of 0.5 °C.

From a present climate change point of view, the reconstruction of large river discharge allows the estimation of global and continental monthly runoffs fluctuations over the last century, providing a new insight into temporal succession of dry and humid periods. These global hydrological signals also highlight the complexity of the hydrological consequences and feedbacks of recent climate changes but still indicate a rough increase of global runoff over the last 75 years with a 15-year shift. Synchronism or temporal shifts between continents are also put in evidence.

A regression between global temperature and runoff suggests that the global runoff increases by 4% when global temperature rises by 1 °C. This trend is in agreement with recent investigations indicating a global increase of precipitation. However, extrapolation of this runoff-temperature relationship to past and future climate constitutes a non-trivial operation essentially because now the ocean reservoir response to climate warming remains also a matter of debate. From our data, it remains difficult to discriminate anthropogenic effects from natural tendencies in global runoff signals [28,41] even if a recent conjugated acceleration of both global temperature and runoff is observed.

The global runoff increase should be qualified at the continental scale where both increasing (North America, Asia, and South America), stability (Europe) and decreasing (Africa) trends have been shown. These unexpected regional heterogeneities reflect the high nonlinearity of the hydrological cycle response to recent climate change.

In conclusion, this contribution provides the first experimental data-based evidence demonstrating the link between the global warming and the intensification of the global hydrological cycle. This corresponds to more intense evaporation over oceans *coupled* to continental precipitation increase or continental evaporation decrease. This process finally leads to an increase of the global continental runoff.

References

[1] Allen MR, Ingram WJ. Constraints on future changes in climate and the hydrological cycle. Nature 2002;419:224–32.

[2] Baumgartner A, Reichel E. The world water balance. Amsterdam: Elsevier; 1975. 179 p.

[3] Berner RA. Atmospheric carbon dioxide levels over Phanerozoic time. Science 1991;1249:1382–6.

[4] Berner RA. GEOCARB II: a revised model of atmospheric CO_2 over Phanerozoic time. Am J Sci 1994;294:56–91.

[5] Berner RA, Kothavala Z. GEOCARB III: a revised model of atmospheric CO_2 over Phanerozoic time. Am J Sci 2001;301:182–204.

[6] Berner RA, Lasaga AC, Garels RM. The carbonate–silicate geochemical cycle and its effect on atmospheric carbon dioxide over the past 100 million years. Am J Sci 1983;283:641–83.

[7] Brady PV. The effect of silicate weathering on global temperature and atmospheric CO_2. J Geophys Res 1991;96:18101–6.

[8] Chahine MT. The hydrological cycle and its influence on climate. Nature 1992;359:373–80.

[9] Compagnucci RH, Blanco SA, Figliola MA, Jacovkis PM. Variability in subtropical Andean Argentinean Atuel river: a wavelet approach. Environmetrics 2000;11:251–69.

[10] Dai A, Trenberth KE, Karl TR. Global variations in droughts and wetspells: 1900–1995. Geophys Res Lett 1998;25(17):3367–70.

[11] Daubechies I. Ten lectures on wavelets. CSBM-NSF Series Appl. Math., No 61. SIAM Publi.; 1992. 357 p.

[12] Dettinger MD, Diaz HF. Global characteristics of stream flow seasonality and variability. J Hydrometeorol 2000;1:289–310.

[13] Doll P, Kaspar F, Alcamo J. Computation of global water availability and water use at the scale of large drainage basins. Math Geol 1999;4:111–8.

[14] Fraedrich K, Jiang J, Gerstengarbe F-W, Werner PC. Multisale detection of abrupt climate changes: application to river nile flood. Int J Clim 1997;17:1301–15.

[15] Gates WL. The numerical simulation of ice-age climate with a global general circulation model. J Atm Sc 1976;33:1844–73.

[16] Ghil M, Allen MR, Dettinger MD, Ide K, Kondrashov D, Mann ME. Advanced spectral methods for climatic time series. Rev Geophys 2002;40(1):1–41.

[17] Goddéris Y, François LM. The Cenozoic evolution of the Strontium and Carbon cycles: relative importance of continental erosion and mantle exchanges. Chem Geol 1995;126:169–90.

[18] Mc Carthy JJ, Canziani OF, Leary NA, Dokken DJ, White KS, editors. IPCC. Climate change 2001—impacts, adaptation and vulnerability. Contribution of working group II to the third assessment report of the intergovernmental panel on climate change. Cambridge, United Kingdom and New York, NY, USA: Cambridge University Press; 2001. 1032 p.

[19] Jones PD, Wigley TML, Wright PB. Global temperature variations between 1861 and 1984. Nature 1986;322:430–4.

[20] Jones PD, Raper SCB, Bradley RS, Diaz H, Kelly PM, Wigley TML. Northern hemisphere surface air temperature variations: 1851–1984. J Clim Appl Meteor 1986;25:161–79.

[21] Jones PD, Raper SCB, Bradley RS, Diaz H, Kelly PM, Wigley TML. Southern hemisphere surface air temperature variations: 1851–1984. J Clim Appl Meteor 1986;25:1213–30.
[22] Jury MR, Melice JL. Analysis of Durban rainfall and Nile river flow 1871–1999. Theoret Appl Clim 2000;67:161–9.
[23] Jury MR, Enfield DB, Mélice JL. Tropical monsoons around Africa: stability of El ninon—southern oscillation associations and links with continental climate. J Geophys Res 2002:107.
[24] Karl TR, Knight RW, Plummer N. Trends in high frequency climate variability in the twentieth century. Nature 1995;377:217–20.
[25] Labat D, Ababou R, Mangin A. Introduction of wavelet analyses in karts hydrogeology: the case of Licq Atherey basin. Ground Water 2001;39(4):605–15.
[26] Labat D, Ababou R, Mangin A. Rainfall runoff relations for karstic springs: continuous wavelet and multiresolution analysis. J Hydrol 2000;238:123–48.
[27] Lafrenieres M, Sharp M. Wavelet analysis of inter annual variability in the runoff regimes of glacial and nival stream catchments, Bow Lake, Alberta. Hydrol Process 2003;17(6):1093–118.
[28] Levitus S, Antonov JI, Wang J, Delwotrh TL, Dixon KW, Broccoli AJ. Anthropogenic warming of Earth's climate system. Science 2001;292:267–70.
[29] Mallat S. A theory for multiresolution signal decomposition: the wavelet representation. IEEE Trans Pat Anal Mach Intell 1989;11:674–93.
[30] Manabe S, Stouffer RJ. Century scale effects of increased atmospheric CO_2 on the ocean–atmosphere system. Nature 1993; 364:215–8.
[31] Manabe S, Stouffer RJ. Sensitivity of a global climate model to an increase of CO_2 concentration in the atmosphere. J Geophys Res 1980;85:5529–54.
[32] Masuda K, Hashimoto Y, Matsuyama H, Oki T. Seasonal cycle of water storage in major river basins of the world. Geophys Res Lett 2001;28(16):3215–8.
[33] Milly PCD, Wetherhald RT, Dunne KA, Delworth TL. Increasing risk of great floods in a changing climate. Nature 2002;42(15):514–7.
[34] Nijssen B, O/Donnell GM, Lettenmaier DP, Lohmann D, Wood EF. Predicting the discharge of global rivers. J Clim 2001; 14:3307–23.
[35] Oki T, Musiake K, Matsuyama H, Masuda K. Global atmospheric water balance and runoff from large river basins. Hydrol Process 1995;9:655–78.
[36] Pekarova P, Miklanek P, Pekar J. Spatial and temporal runoff oscillation analysis of the main rivers of the world during the 19th–20th centuries. J Hydrol 2003;274(1):62–79.
[37] Pierrehumbert RT. The hydrologic cycle in deep-time climate problems. Nature 2002;419:191–8.
[38] Probst JL, Tardy Y. Global runoff fluctuations during the last 80 years in relation to world temperature change. Am J Sci 1989;289:267–85.
[39] Probst JL, Tardy Y. Long range streamflow and world continental runoff fluctuations since the beginning of this century. J Hydrol 1987;94:289–311.
[40] Schlesinger ME, Ramankutty N. An oscillation in the global climate system of period 65–70 years. Nature 1994;367: 723–6.
[41] Stott PA et al. External control of 20th century temperature by natural and anthropogenic forcings. Science 2000;290:2133–6.
[42] Vörösmarty CJ, Fekete BM, Tucker BA, Global river discharge database (RivDis) v. 1.1. Available from: http://www-eosdis.ornl.org; 1998.
[43] Vörösmarty CJ, Green P, Salisbury J, Lammers RB. Global water resources: vulnerability from climate change and population growth. Science 2000;289:284–8.
[44] Walker JCG, Hays PB, Kasting JF. A negative feedback mechanism for the long-term stabilization of Earth's surface temperature. J Geophys Res 1981;86:9776–82.